Building and Environment, Vol. 25, No. 2, pp. 85–94, 1990.
Printed in Great Britain.

0360–1323/90 $3.00 + 0.00

Modelling of Moisture Transfer in Structures—II. A Comparison of a Numerical Model, an Analytical Model and some Experimental Results

M. J. CUNNINGHAM*

The results of comparing the predictions of an analytical and a numerical model against experimental data on the moisture performance of four flat roofs is presented. The experimental data was obtained by placing one metre square roof specimens between two controlled climate chambers and subjected them to steady-state driving conditions. The agreement with the experimental data shown by both models is good, the numerical model showing the ability to follow fine detail in the moisture behaviour. The results suggest that the concepts rising from the analytical model are useful ones, and that the numerical model should perform well under field conditions.

INTRODUCTION

IT IS WIDELY accepted that an important route towards an understanding of the moisture performance of structures, leading to better design tools, is via mathematical modelling of these systems. In a companion paper [1], a numerical model was described for predicting the moisture performance of structures. The author has also described an analytical approach to understanding moisture transfer in structures [2], developed to describe moisture performance with a small number of parameters, each with clear physical meaning. This paper is concerned with comparing the predictions of the numerical and the analytical models with experimental data obtained from one metre square flat roof specimens placed between controlled climate chambers [3] under steady-state conditions. The results represent the first step in a validation process for the numerical model, and an investigative process for the analytical model, to ascertain its range of validity, and the usefulness of the concepts arising from it. Full confidence in the validity of the numerical model will require its predictions to be tested against data obtained from specimens subjected to cyclic conditions, with air leakage, and also against data obtained from real buildings [4].

This paper begins by summarising the details of the analytical model, including further details that must be added to it if there are condensation processes taking place within the structure, or if the details of the structure are not quite identical to those assumed in the construction of the analytical model. The details of the experiments performed are then summarised. Finally the results showing the comparison between the experiments, and the analytical and numerical models are presented and the significance of these discussed.

* BRANZ, Private Bag, Porirua, New Zealand.

SUMMARY OF THE ANALYTICAL MODEL

The details of the numerical model are contained in a companion paper [1], and will not be repeated here. This section summarises the analytical model, full details of which can be found in reference [2]. Refer to [1] and [2] for nomenclature used in this work.

The geometry considered by the analytical model consists of a flat roof or wall with a hygroscopic framing material which is joined to the inside and outside linings, and an associated cavity filled with insulation or air, see Fig. 1. This geometry is modelled as two nodes, one being the framing material and the other the cavity.

The differential equations governing conservation of mass are written down for each node. To solve the resulting pair of differential equations requires a connection to be given between the vapour pressures p (Pa) and the moisture concentrations m (kg m^{-3}) in the structure. Physically this connection is described by the sorption curve of the material in question, and the behaviour of vapour pressure with temperature. The analytical model makes the connection:

$$p = km, \tag{1}$$

and assumes that k is constant. This linearises the sorption curve, but more importantly ignores temperature effects and as such is the most severe approximation made in the analytical model.

With this approximation, the equations can be solved for a variety of driving conditions. For steady driving conditions, the solutions show that, after an initial tran-

BAE 25:2-A

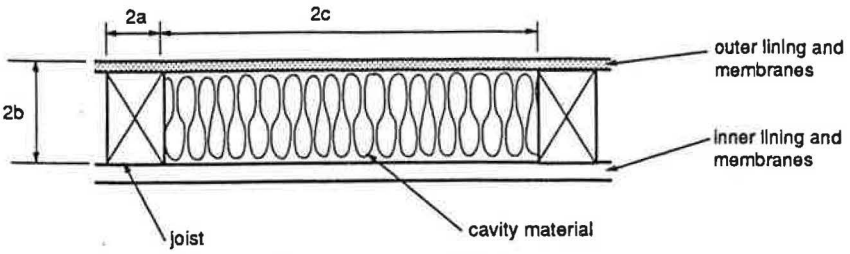

Fig. 1. Diagram of structure type modelled by the analytical model.

sient, while the moisture content of the framing material is above fibre saturation (fsp) the moisture content of the framing material falls at a constant rate, and once the moisture content of the framing material is below fsp, the vapour pressure and the moisture content of the framing material falls exponentially.

Specifically, above fsp the analytical model predicts a drying rate of the framing material given by:

$$\frac{dm_w}{dt} = -\frac{1}{V_w}\left(\frac{p_w - \bar{p}_o}{R_{ae}} + \frac{p_w - \bar{p}_w}{R_{be}}\right), \tag{2}$$

while below fsp, the framing material dries according to the expression:

$$m_w = A\, e^{-t/t_2} + \underline{m}_w. \tag{3}$$

R_{ae} and R_{be} here are lumped vapour flow resistances depending on the paths available for moisture transfer out of the framing material.

$\bar{p}_o$ and $\bar{p}_w$ are the external driving vapour pressures suitably weighted by expressions involving vapour flow resistances and air leakage rates according to their net influence on the structure. $\bar{p}_o$ for example is given by:

$$\bar{p}_o = R_{oe} \sum_{i=1}^{2} \left(\frac{A_{io}}{r_{io}} + \frac{V_o F_{io} W}{RT}\right) p_i. \tag{4}$$

Definitions for the terms in equation (4) appear in [2]. In equation (3), A is determined by the initial conditions while $\underline{m}$ is the steady-state value of the framing material moisture concentration given by:

$$\underline{m}_w = \frac{R_{ae}\bar{p}_w + R_{be}\bar{p}_o}{k_w(R_{ae} + R_{be})},$$

and t_2 is the time-constant governing the rate of drying of the hygroscopic material. Its value is given by the expression:

$$\frac{1}{t_2} = \frac{1}{t_a(1+\gamma)} + \frac{1}{t_b(1+\delta)}, \tag{5}$$

where γ and δ are ratios of vapour flow resistances for the drying of the unenclosed framing material to the drying of enclosed framing material while t_a and t_b are drying rates through the side and top faces of the unenclosed framing material. The net unenclosed drying time-constant for the framing t_w is given by:

$$\frac{1}{t_w} = \frac{1}{t_a} + \frac{1}{t_b}.$$

Full definitions and expressions for the above terms can be obtained in [2].

Equation (5) is the key result of the analytical model in that it shows how the drying time of the framing material once enclosed in the structure is increased over the unenclosed drying time, according to the air and vapour tightness construction details of the structure and the driving forces upon it. Furthermore, earlier work [5] showed that, given t_2, the moisture behaviour of the structure can be predicted for any time behaviour of the driving forces, insofar as k in equation (1) can be taken as approximately constant.

Certain modifications and additions must be made to the analytical model as described in reference [2], firstly to handle the presence of condensation, and secondly to handle a geometry which is not quite that for which the model was developed.

The presence of condensate on the cavity walls is handled in the same way as in reference [5] where it was shown how to analyse a building cavity containing an evaporating/condensing water surface. An extra term must be added to the mass balance equation for the cavity since the flow of moisture J (kg s^{-1}) from a condensation layer to the cavity will be given by:

$$J = Ah(p_{sat} - p_o),$$

where h is the surface mass transfer coefficient (kg N^{-1} s^{-1}) and p_{sat} is the saturated vapour pressure over the condensation.

This will have the effect of modifying the expression for the driving vapour pressure on the cavity, $\bar{p}_o$, in equation (4) to become:

$$\bar{p}_o = R_{oe}\left(\sum_{i=1}^{2}\left(\frac{A_{io}}{r_{io}} + \frac{V_o F_{io} W}{RT}\right) p_i + Ahp_{sat}\right)$$

where the expression for R_{oe} given in reference [2], is now given by:

$$\frac{1}{R_{oe}} = \sum_{i=1}^{2}\left(\frac{A_{io}}{r_{io}} + \frac{V_o F_{oi} W}{RT}\right) p_i + Ah.$$

These modified expressions for the driving vapour pressure on the cavity, $\bar{p}_o$, and for R_{oe}, are then used in the various expressions of the analytical model given in reference [2].

In practice the mass transfer coefficient h which is of the order 10^{-8} kg N^{-1} s^{-1}, can be much larger than the other terms, particularly if air change rates into the cavity are low. In this case, R_{oe} in the presence of condensation can be approximated by:

$$R_{oe} \simeq \frac{1}{Ah}.$$

With this approximation $\bar{p}_o$ becomes:

$$\bar{p}_o \simeq p_{sat}. \quad (6)$$

This approximation highlights the fact that in tight cavities condensation has a dominating influence on the vapour pressure within the cavity.

Two of the experimental samples described below are twin cavity structures, whose geometry is not that around which the analytical model is based. However, for these particular samples it is adequate to treat the top cavity and its framing material acted upon by above-roof climate forces as one system, and the bottom cavity and its framing system acted upon by the below-ceiling climate forces plus the forces from the top cavity as a second system. Each of these systems conforms to the two-node geometry of the analytical model. More details describing the application of the analytical model to these samples can be found below.

DETAILS OF THE EXPERIMENTS PERFORMED

Full details of the experiments performed can be found in reference [3]. In this section they will be summarised briefly as follows.

Four runs were conducted. In each run, a one metre square flat roof specimen was placed between controlled climate chambers [3] under steady state conditions. There were two main specimen types (see Fig. 2), the first having a 150 mm cavity, half-filled with fibre-glass insulation, a corrugated profile metal roof cladding over building paper, and a (nominal) 50 × 150 mm timber joist; the second having a 50 mm lower cavity bounded at the top by building paper, filled with fibre-glass insulation and containing a 50 × 50 mm joist, with an external cladding of concrete tiles placed on 25 × 50 mm tile battens. The gap between the building paper and the tiles produced by the tile battens created a second upper cavity. Ceiling linings in both cases were gypsum plaster board. Each specimen had a central timber joist that was soaked in water prior to the run to give a high initial moisture content.

Details of each run are as follows.

Run (1). The metal clad, single cavity specimen was used with a foil backing to the gypsum plaster board to create a vapour barrier. It was driven with conditions below the ceiling established at a steady state value of 18°C and 65% RH (nominal) and conditions above the roof of 4°C and 80% RH (nominal).

Run (2). The same metal clad specimen was used without the vapour barrier and run with the same conditions below the ceiling, but with conditions above the roof of 25°C and 57% RH.

Run (3). The concrete tile, twin cavity specimen was run with foil backed gypsum plaster board and the same nominal below-ceiling conditions of 18°C and 65% RH, and above-roof conditions of 25°C and 57% RH.

Run (4). The concrete tile specimen was run without a vapour barrier, with the same conditions below the ceiling, but with conditions above the roof of 4°C and 80% RH.

The driving conditions are summarised in Table 1.

All specimens were constructed to be quite airtight, so that diffusion became the dominant moisture transfer mechanism. Details of the relative size of diffusion and residual air leakage are to be found in reference [3].

Instrumentation used on the specimens is reported in [3]. For the purposes of this work, the moisture probes were the most important instrumentation. These probes consisted of 10 × 10 mm gold plated brass squares embedded in the timber, spaced 5 mm apart. DC resistance and AC impedance was measured across these probes, and a per cent moisture content by weight calculated using a procedure given in [6]. The location of the relevant probes is shown in Fig. 3. For the timber member as a whole, mean moisture contents were calculated by taking a weighted mean of each probe measurement, according to the estimated proportion of the joist each probe was measuring. It was shown in reference [6] that these probes give good accuracy below 25–30% moisture content, but become increasingly inaccurate at higher moisture contents. The raw moisture probe readings were taken each two hours by a HP3497 data logger and HP3456 DVM and passed on *via* an IEEE bus to a PDP-11/24 computer where moisture contents were calculated online and stored for future use.

INPUT DATA TO THE MODELS

Each model was used to calculate the transient response of the specimen, from the initial conditions established, to the constant boundary conditions imposed at the top and bottom of the specimen.

Figure 4 shows the nodes used in the numerical calculations. Runs (1) and (2) are modelled two-dimensionally, but runs (3) and (4) have a three-dimensional factor, in that the tile batten runs at right angles to the main joist and has a depth of 50 mm whereas all other components have a depth of 1 m.

Table 2 contains the values of diffusion coefficient and conductivity used for the various materials making up the specimens. The value of 4.9×10^{-14} s for the diffusion coefficient of the metal is an effective value, chosen to give a vapour flow resistance of 20.3 GN s kg^{-1} in agreement with that measured by experiment. (The vapour flow resistance is not larger than this because of overlaps in the metal sheets.)

It was explained in the previous paper [1] that the numerical model uses vapour pressure as a driving poten-

Table 1. Specimen driving conditions

Run	Below specimen Temp. (°C)	Below specimen RH (%)	Above specimen Temp. (°C)	Above specimen RH (%)
(1)	18	65	4	80
(2)	18	65	25	57
(3)	18	65	25	57
(4)	18	65	4	80

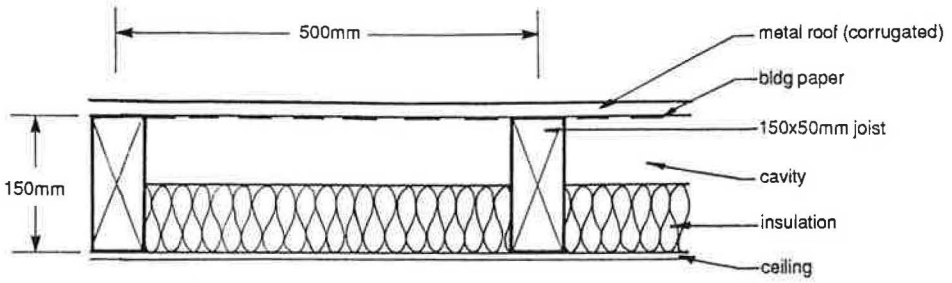

(a) First specimen type

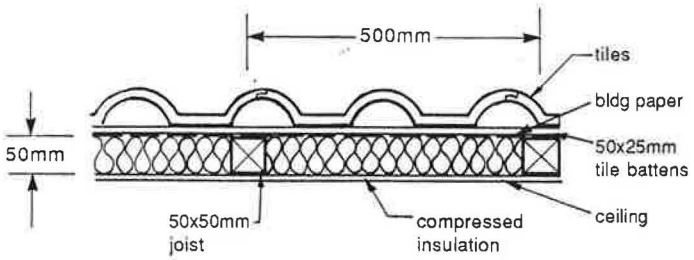

E - W Section

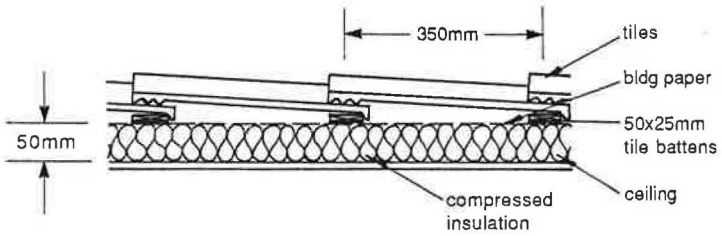

N - S Section

(b) Second specimen type

Fig. 2. Cross sections of the experimental specimen types.

tial for moisture transfer, both below and above fsp. Above fsp an effective vapour diffusion coefficient must be used that compensates for the very small vapour pressure differences met with in this region, and gives the correct mass transfer rate. In fact, the correct mass transfer rates are not well known at these moisture contents [7], and in the context of the durability of structures, one would require that moisture contents were not at these levels for long periods of time. Figure 5 shows the vapour diffusion coefficient chosen for the timber as a function of moisture content. Choosing this variation in the diffusion coefficient above fsp has been done merely to give good agreement with results above fsp, and as such is the least satisfactory aspect of the modelling described here; however, as explained above, the present state of knowledge makes this kind of approach inevitable. No such function was required for the other materials in the specimen since they did not become wet enough.

In the numerical model, moisture contents corresponding to a given relative humidity (as determined by vapour pressure and temperature) were found using the sorption formula given in [8], viz:

$$\ln(mc) = A + B\ln((0.01\phi)^{-c} - 1), \qquad (7)$$

where: A, B and c are constants characterising the material; mc is the moisture content of the material as a % (kg/kg); ϕ is the associated relative humidity (%).

Cunningham [8] gives separate curves and associated

Table 2. Values used for material coefficients

Material	Vapour diffusion coefficient (s)	Thermal conductivity ($w\ m^{-1}\ °C^{-1}$)
Wood	1.5×10^{-11}	0.18
Plasterboard	3.0×10^{-11}	0.22
Fibreglass batts	2.0×10^{-10}	0.05
Concrete tiles	2.0×10^{-11}	1.0
Steel*	4.9×10^{-14}	51.0

* See text.

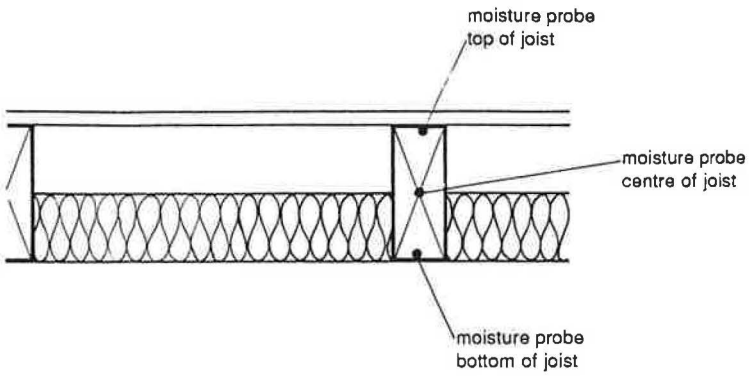

(a) First specimen type

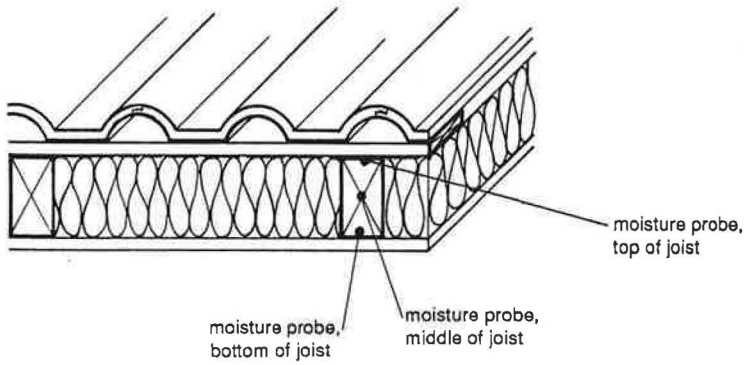

(b) Second specimen type

Fig. 3. Location of sensors.

parameters for sorption and desorption; since the experiments were all concerned with the drying of the framing timbers, the desorption form of the curve was used.

The analytical model requires values for t_a and t_b, the drying rates through the side and top faces of the unenclosed framing material. These values were found using the numerical model on unexposed framing material of appropriate dimensions, and a diffusion coefficient of 1.5×10^{-11} s as indicated in Table 2.

The twin cavity systems of runs (3) and (4) require special treatment when using the analytical model. As explained earlier, the top cavity and its framing material acted upon by above-roof climate forces are taken as one system, and the bottom cavity and its framing system acted upon by the below-ceiling climate forces plus the forces from the top cavity are taken as a second system. Formulae (2) and (3) are used on the top cavity and its framing material using appropriate approximate values of $\bar{p}_o$ and $\bar{p}_w$, and, from the vapour pressure thus calculated in the top cavity, fresh values of $\bar{p}_o$ and $\bar{p}_w$ are calculated to act as driving forces on the lower cavity. The lower cavity containing the structural joist is both larger and more important in the moisture performance of the structure, and receives more accurate modelling using the scheme outlined.

In run (3), because the presence of the vapour barrier means that vapour pressures below the ceiling do not strongly influence vapour pressures in the top cavity, $\bar{p}_o$ and $\bar{p}_w$ can be calculated approximately using vapour pressures above the roof only. In this case the batten in the top cavity was predicted by the analytical model to fall below fsp after about 20 days. After this, the analytical model predicts an exponential drop in the top cavity vapour pressure conditions, with a time constant of 10 h, to a vapour pressure roughly equal to the above-roof driving vapour pressure. Hence, in analysing conditions in the lower cavity, values of $\bar{p}_o$ and $\bar{p}_w$ are different before and after 20 days; this shows as a discontinuity in slope of the analytical predictions for run (3), see Fig. 6(c). The numerical model shows this slope change at about 14 days, and there is also a hint of this slope change in the experimental data at around 10–12 days.

In run (4), vapour pressures and temperatures are such that condensation appears on the concrete tiles; consequently formula (6) is used to calculate the top cavity vapour pressure which remains constant throughout the

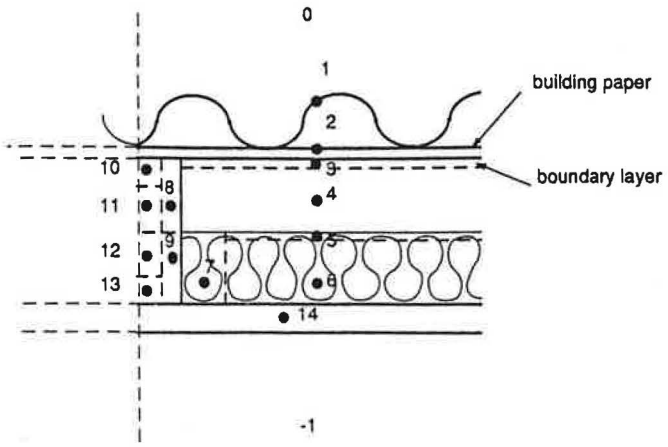

(a) First specimen type

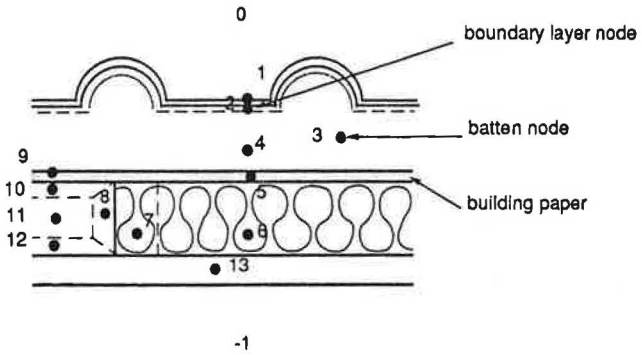

(b) Second specimen type

Fig. 4. Nodal structure of specimens.

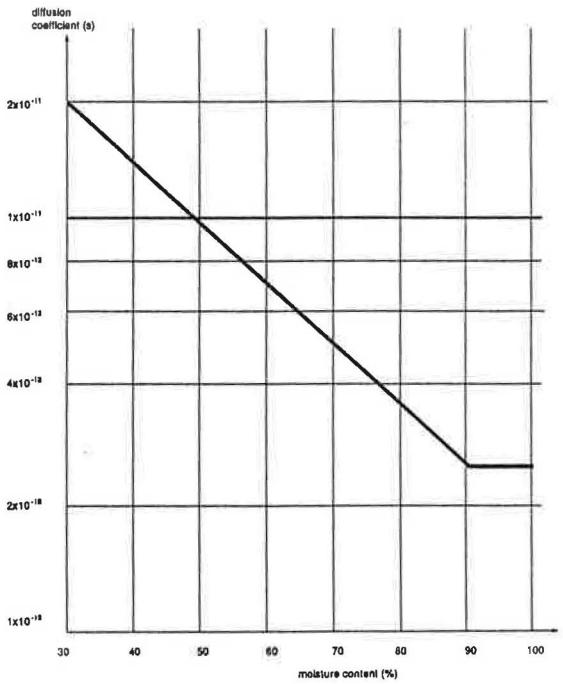

Fig. 5. Vapour diffusion coefficient of timber above fibre saturation as used by the numerical model.

run. This condition, together with the conditions below the ceiling, were used in equations (2) and (3) as the driving forces on the bottom cavity to yield the results shown in Fig. 6.

COMPARISON BETWEEN EXPERIMENTAL AND MODELLED RESULTS

In these steady-state experiments the models are concerned with rates of drying, with the analytical model predicting linear drying above fsp, and exponential drying below it. In order to show to the eye the accuracy (or otherwise) of the rates of drying predicted by the models, the time at which the experimental data show that the joist has dried to fsp is used as the reference point in determining the initial conditions used. For the analytical model, exponential drying rates are graphed forward from that time, and linear drying rates are graphed backwards; while for the numerical model small adjustments were made in the initial moisture contents used in the model, so that the predicted results passed through the experimental result at fsp. It must be remembered that the experimental data for moisture contents above fsp are not highly accurate, and the small deviations from the initial moisture contents used are within experimental error.

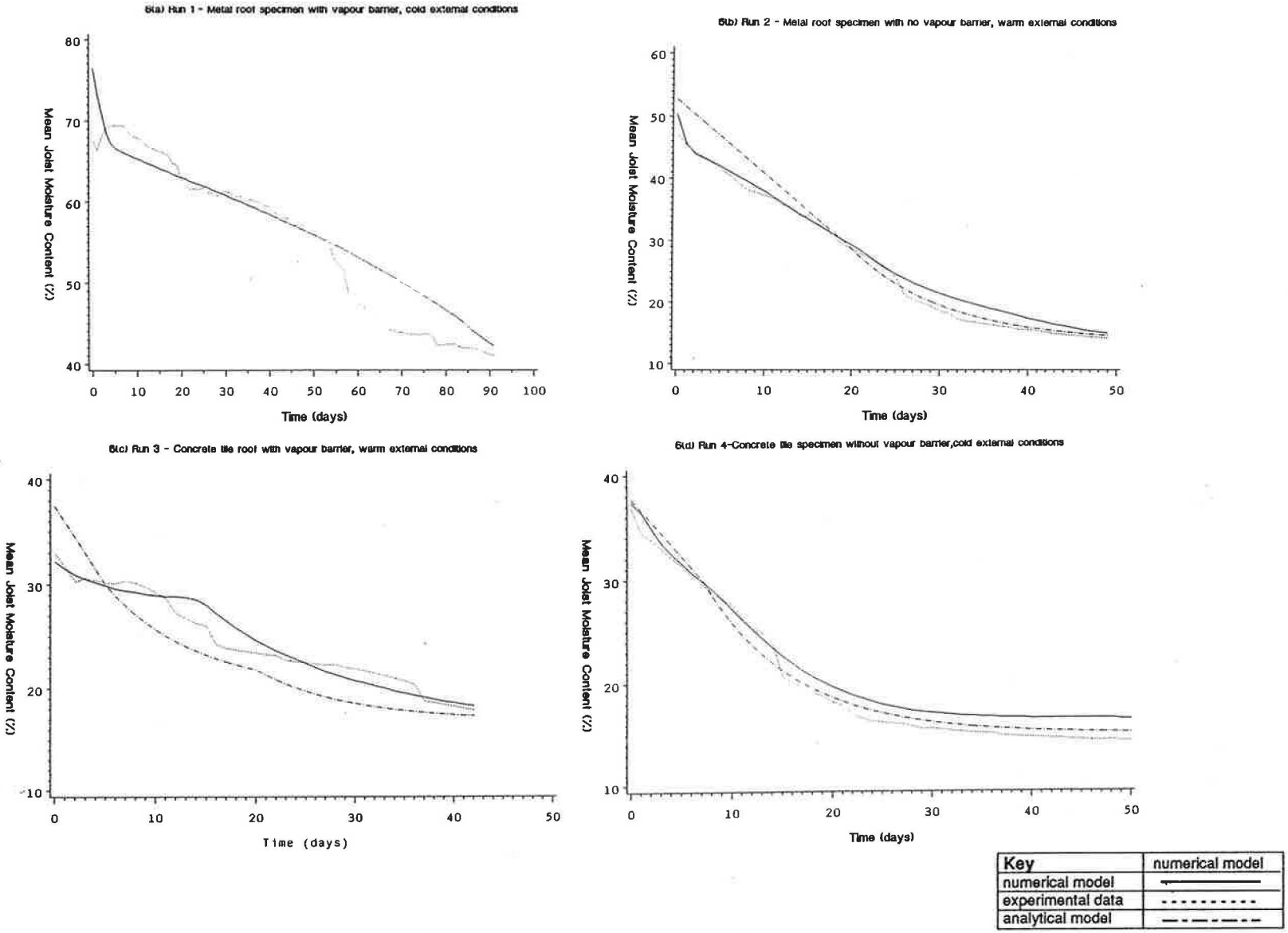

Fig. 6. Comparison between modelled and experimental mean joint moisture contents.

Figure 6 shows the comparison between the experimental and modelled results, both numerical and analytical, for the mean moisture content for each run, while Fig. 7 shows the results for each individual probe. (As described in [3], the accuracy of the experimental data for the moisture contents is $\pm 1\%$ moisture content below 15% moisture content rising to $\pm 10\%$ moisture content at 40% moisture content. Beyond 50% moisture content the experimental data is indicative only.) No analytical results are shown for run 1 (cold out-door conditions, vapour barrier, and impermeable metal roof cladding) because the conditions encountered here are beyond the reach of the analytical model. Cladding vapour resistances are very high and not well known experimentally. Moisture contents are well above fsp and therefore also not known well experimentally. Large temperature gradients exist within the structure, which are not modelled by the analytical model. In all, the conditions are extreme and beyond the reach of the analytical model. This is also a difficult region for the numerical model particularly since transport properties are not well known there (as explained above), and indeed the numerical model predictions for run 1 are better than expected.

The mean moisture content results taken as a set, show very encouraging agreement with the experimental results, both for the analytical and numerical models. The predictions for the individual probes provide a more demanding test for the numerical model. Perfect agreement cannot be expected here, because detailed knowledge of the moisture driving potentials does not exist, particularly under strong temperature gradients, and because the experimental results at higher moisture contents are subject to large errors. Nevertheless, agreement here is fair to good except for the case of the moisture content at the bottom of the joist in run (1). This discrepancy is thought to be due to corrosion of the very thin foil (7 microns thick) under the joist, hastened by the high moisture content of the joist, and subsequent movement of timber moisture into the gypsym plaster board.

The moisture probes close to the surface are not weighted heavily in calculating the mean moisture content; therefore the accuracy of prediction of surface moisture content does not significantly affect the accuracy of prediction of mean moisture content. It is clear that all the main features of the internal moisture transfers have been captured by the numerical model, as evidenced by the ability of the numerical model to reproduce most of the features that appear in the experimental data.

Experimentally, condensation was observed in runs (1) and (4). It is difficult to quantify amounts of condensate experimentally, but attempts were made by weighing components of the specimen while still wet immediately after the runs were finished. It is also difficult to calculate the rate of accumulation of condensation with the analytical model as this requires an accurate knowledge of condensation and cavity vapour pressures. For run (1) the numerical model predicts an accumulation of moisture in the building paper to very high levels. In practice, building paper can hold water quantities up to in the order of 100 g m^{-2} without dripping. This level is predicted to be reached after 72 days. Condensation as such is predicted below the building paper after 87 days. After that condensation in and below the building paper continues to accumulate with a total condensate of 1200 g m^{-2} predicted after 100 days. This agrees well with the experimental estimate of at least 1100 g m^{-2}. For run (4) the numerical model predicts a rate of condensation of about 36 g m^{-2} day^{-1} for a total condensate at the end of 50 days of 1800 g m^{-2}. The experimental estimate was of at least 600 g m^{-2}.

The good agreement between experimental data and the predictions of the analytical model is very encouraging, but perhaps not too surprising. The most severe approximation made in order to solve the differential equations of the two node analytical model, was to assume that k is constant in equation (1) above. As the experiments are steady-state, this approximation is well met. Cyclic conditions, in which temperature and hence k will change with time will provide a much more severe test of the analytical model.

On the other hand, these experiments must be seen as providing a very good test of the numerical model. If conditions were cyclic as they will be in the field (and later experiments), strong temperature gradients will not be imposed for long periods of time, and averaging effects will appear in the results. Consequently the numerical model would not be called upon to predict performance under more extreme conditions where transport properties are less well known. The numerical model has performed very well under quite difficult conditions which suggests that it should handle field conditions quite satisfactorily.

CONCLUSIONS

The results of comparing the predictions of an analytical model, and a numerical model, against some experimental data of the moisture performance of some flat roofs have been presented. Both models agree well with the experiments, with the numerical model showing the ability to reproduce some quite fine detail in the experimental data. Present knowledge makes it difficult to give a good treatment of moisture performance above fsp (and indeed, most models do not attempt to do so) but fortunately, practical considerations imply that high accuracy in this region is not required.

It is felt that the data set presents a quite severe test of the numerical model, but a relatively forgiving test of the analytical one. Despite the fact that the analytical model cannot be said to have been subjected to a rigorous test, its performance here is more than good enough to justify the validity and usefulness of the concepts that have grown out of it, in particular the idea of associating a time constant with the rate of drying of construction moisture, and then ascertaining quantitatively how this time constant is increased once the framing is enclosed.

Full confidence in the validity and usefulness of the models will require model predictions to be tested against data obtained from specimens subjected to cyclic conditions, with air leakage, and their predictions to be tested against data obtained from real buildings.

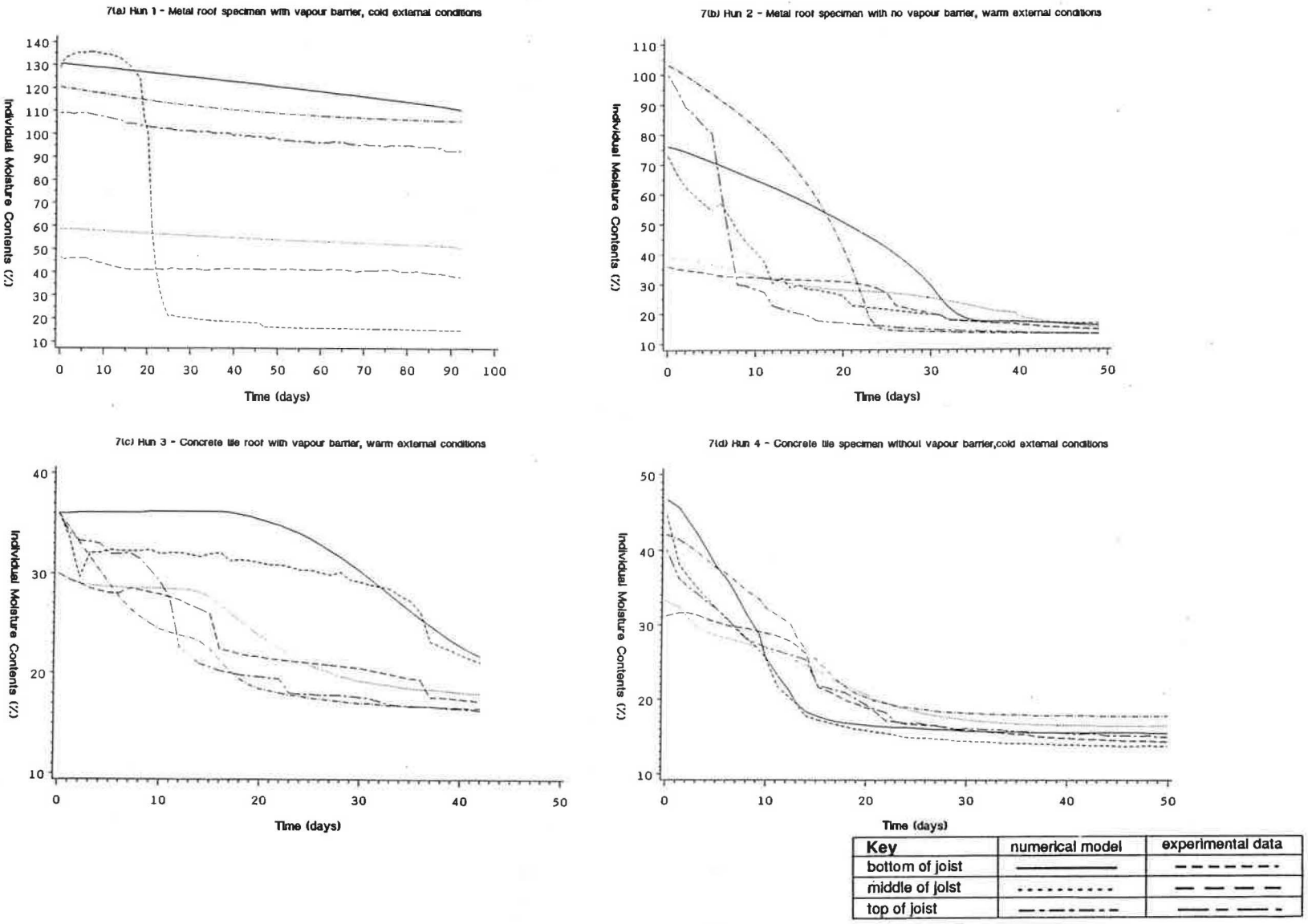

Fig. 7. Individual moisture contents.

REFERENCES

1. M. J. Cunningham, Modelling of moisture transfer in structures—I. A description of a finite-difference nodal model. *Bldg Envir.* **25**, 55–61 (1990).
2. M. J. Cunningham, The moisture performance of framed structures—a mathematical model. *Bldg Envir.* **23**, 123–125 (1988).
3. M. J. Cunningham, Drying of construction moisture in timber framed flat roofs. I. Low air leakage. *ASHRAE Trans. II* **93**, 153–170 (1987).
4. Research programme of work 1988–89. Building Research Association of New Zealand, Judgeford (1988).
5. M. J. Cunningham, Further analytical studies of building cavity moisture concentrations. *Bldg Envir.* **19**, 21–29 (1984).
6. M. J. Cunningham, Automatic datalogging timber moisture contents over the range 10–15% w/w. *ISA Trans.* **25**, 73–80 (1986).
7. M. J. Cunningham, R. B. Keey and C. Kerdemelidis, Isothermal moisture transfer coefficients in Pinus radiata above the fibre-saturation point using the moment method. *Wood Fiber Science* **21**, 112–122 (1989).
8. M. J. Cunningham and T. J. Sprott, Sorption properties of New Zealand building materials. Research report R43, Building Research Association of New Zealand, Judgeford (1984).